Article

Suppression of black-hole growth by strong outflows at redshifts 5.8–6.6

https://doi.org/10.1038/s41586-022-04608-1

Received: 23 September 2021

Accepted: 3 March 2022

Published online: 11 May 2022

Check for updates

M. Bischetti[1]✉, C. Feruglio[1,2], V. D'Odorico[1,2,3], N. Arav[4], E. Bañados[5], G. Becker[6], S. E. I. Bosman[5], S. Carniani[3], S. Cristiani[1], G. Cupani[1], R. Davies[7,8], A. C. Eilers[9], E. P. Farina[10], A. Ferrara[3], R. Maiolino[11], C. Mazzucchelli[12], A. Mesinger[3], R. A. Meyer[5], M. Onoue[5], E. Piconcelli[13], E. Ryan-Weber[7,8], J.-T. Schindler[5], F. Wang[14], J. Yang[15], Y. Zhu[6] & F. Fiore[1,2]

Bright quasars, powered by accretion onto billion-solar-mass black holes, already existed at the epoch of reionization, when the Universe was 0.5–1 billion years old[1]. How these black holes formed in such a short time is the subject of debate, particularly as they lie above the correlation between black-hole mass and galaxy dynamical mass[2,3] in the local Universe. What slowed down black-hole growth, leading towards the symbiotic growth observed in the local Universe, and when this process started, has hitherto not been known, although black-hole feedback is a likely driver[4]. Here we report optical and near-infrared observations of a sample of quasars at redshifts $5.8 \lesssim z \lesssim 6.6$. About half of the quasar spectra reveal broad, blueshifted absorption line troughs, tracing black-hole-driven winds with extreme outflow velocities, up to 17% of the speed of light. The fraction of quasars with such outflow winds at $z \gtrsim 5.8$ is ≈2.4 times higher than at $z \approx 2$–4. We infer that outflows at $z \gtrsim 5.8$ inject large amounts of energy into the interstellar medium and suppress nuclear gas accretion, slowing down black-hole growth. The outflow phase may then mark the beginning of substantial black-hole feedback. The red optical colours of outflow quasars at $z \gtrsim 5.8$ indeed suggest that these systems are dusty and may be caught during an initial quenching phase of obscured accretion[5].

We studied the early growth of supermassive black holes and their feedback on the host galaxies in 30 bright quasars at $z = 5.8$–6.6, with median absolute magnitude $M_{1,450Å} = -26.9$ (−27.8 to −26.2). To this purpose, we exploited homogeneous, wide-band optical and near-infrared (NIR), medium-resolution spectroscopic data with a high signal-to-noise (S/N) ratio from the ultimate X-shooter legacy survey of quasars during reionization (XQR-30).

Black-hole-driven outflows in quasars can be observed as broad (greater than 2,000 km s^{-1}) absorption line (BAL) features in the rest-frame UV spectrum[6], bluewards of prominent emission lines. We systematically searched for absorption troughs associated with the main UV transitions of C IV, Si IV, N V and Mg II ions, accessible through the X-shooter spectra. We modelled the intrinsic, rest-frame UV continuum by constructing composite templates based on Sloan Digital Sky Survey (SDSS) quasar spectra[7,8], matching the continuum slope and the equivalent width of the C IV emission line of each XQR-30 spectrum. Normalized XQR-30 spectra were obtained by dividing each X-shooter spectrum by its matched composite, SDSS template (see Methods and Fig. 1). We measured the balnicity index[6,7] (BI_0, equation (1) in the Methods), which is a modified equivalent width of the BAL absorption.

We identified 14 XQR-30 BAL quasars (Extended Data Table 1), corresponding to a BAL fraction of 47^{+14}_{-13}% (90% confidence level[9]). By conservatively excluding three quasars at $z \approx 6.0$, for which the BAL absorption falls in a spectral region where systematic uncertainty is larger (Methods), the BAL fraction is 41^{+16}_{-14}%. Previous works collecting heterogeneous spectroscopic samples of $z \gtrsim 5.7$ quasars reported a BAL fraction of 16–24% (refs. [10–12]). These values may be considered as lower limits on the actual BAL fraction, as they are typically based on spectra with a resolution and/or S/N ratio lower than those in this work, sometimes limited to a small velocity range $v_{lim} \lesssim 10{,}000$ km s^{-1} (Methods) and mostly determined by visual inspection.

A BAL fraction of 40–50% is substantially higher than the fraction of 10–17%, typically observed in $z \approx 2$–4 quasars[7,13,14]. The observed BAL fraction is the result of an intrinsic BAL distribution convolved with quasar selection criteria. Rather than trying to estimate intrinsic BAL fractions through a redshift-dependent correction, which implies a factor of a few uncertainties, we compare the observed XQR-30 BAL fraction with that observed in quasars at different redshifts with matched rest-frame optical selection criteria, which minimizes the correction factor and thus the connected uncertainty (Methods). As the XQR-30 sample has been selected using the rest-frame optical

[1]INAF - Osservatorio Astronomico di Trieste, Trieste, Italy. [2]IFPU - Institute for Fundamental Physics of the Universe, Trieste, Italy. [3]Scuola Normale Superiore, Pisa, Italy. [4]Department of Physics, Virginia Tech, Blacksburg, VA, USA. [5]Max-Planck-Institut für Astronomie, Heidelberg, Germany. [6]Department of Physics & Astronomy, University of California, Riverside, CA, USA. [7]Centre for Astrophysics and Supercomputing, Swinburne University of Technology, Hawthorn, Victoria, Australia. [8]ARC Centre of Excellence for All Sky Astrophysics in 3 Dimensions (ASTRO 3D), Canberra, Australian Capital Territory, Australia. [9]MIT Kavli Institute for Astrophysics and Space Research, Cambridge, MA, USA. [10]Max Planck Institut für Astrophysik, Garching bei München, Germany. [11]Kavli Institute for Cosmology, University of Cambridge, Cambridge, UK. [12]European Southern Observatory, Vitacura, Chile. [13]INAF - Osservatorio Astronomico di Roma, Monte Porzio Catone, Italy. [14]Department of Astronomy, University of Arizona, Tucson, AZ, USA. [15]Steward Observatory, University of Arizona, Tucson, AZ, USA. ✉e-mail: manuela.bischetti@inaf.it

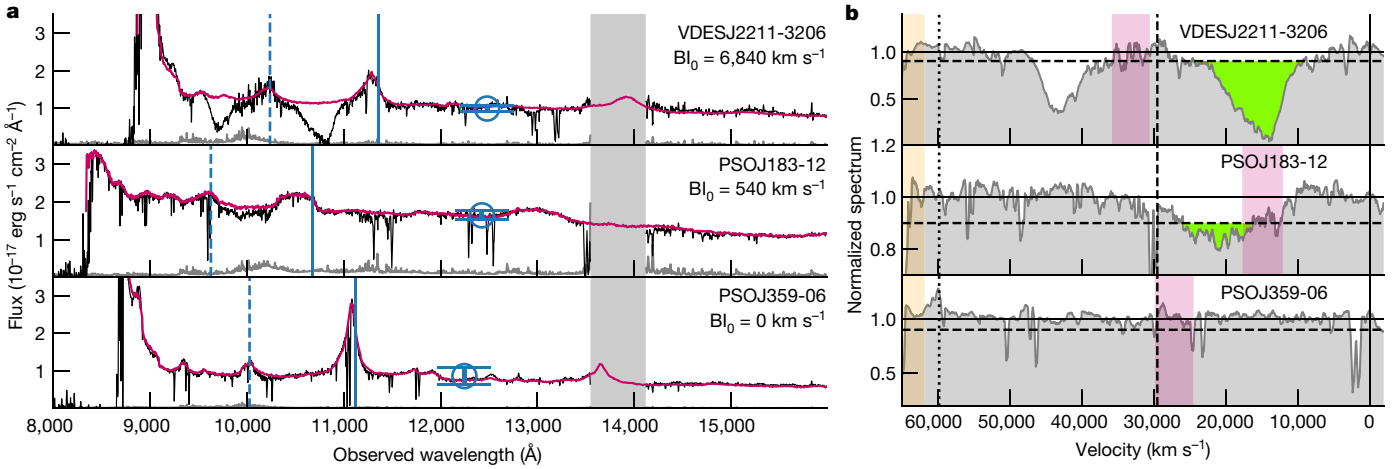

Fig. 1 | X-shooter data, composite templates and normalized spectra. **a**, Examples of X-shooter spectra of XQR-30 quasars (black curves) showing strong ($BI_0 > 1{,}000$ km s^{-1}), weak ($BI_0 < 1{,}000$ km s^{-1}) and no ($BI_0 = 0$ km s^{-1}) BAL absorption features. Spectra have been re-binned to three pixels and the flux uncertainty, multiplied by a factor of five, is shown in grey. The composite template, used to estimate the intrinsic quasar emission, is indicated by the magenta curve. The vertical solid (respectively, dashed) line corresponds to the position of the C IV (respectively, Si IV) emission line according to z_{MgII}. The grey shaded area identifies the spectral window affected by strong telluric absorption. Blue circles represent J-band magnitudes and their associated uncertainties (vertical error bars). **b**, Corresponding normalized spectra, rebinned to 500 km s^{-1}. The velocity axis in each panel is relative to the rest-frame wavelength of C IV. The vertical solid, dashed and dotted lines indicate the position of C IV, Si IV and N V, respectively. The magenta area highlights the overlapping spectral region between the X-shooter Vis and NIR arms in which the uncertainty on the X-shooter response curve is larger (Methods), and orange areas indicate the spectral region affected by substantial intergalactic medium absorption. BAL systems are highlighted as green shaded areas.

colours, we built a control sample of quasars from SDSS at $2.1 < z < 3.2$, requiring a detection in NIR bands, which probe similar rest-frame spectral regions at these redshifts. We searched for BAL quasars in the SDSS control sample using the same identification method used for XQR-30 quasars and measured a BAL fraction of $19.4^{+1.3}_{-1.1}$%, which is 2.4 (1.7–3.3, 90% confidence level) times lower that the fraction at $z \simeq 5.8$–6.6 (Fig. 2). We applied several statistical tests all showing significant differences between the BAL fractions of XQR-30 and the SDSS $z \simeq 2$–3 control samples (see Methods for details).

We verified that the BAL fraction in the SDSS control sample does not significantly vary with the *S/N* ratio of the spectra, consistently with previous studies[7]. The BAL fraction also does not significantly

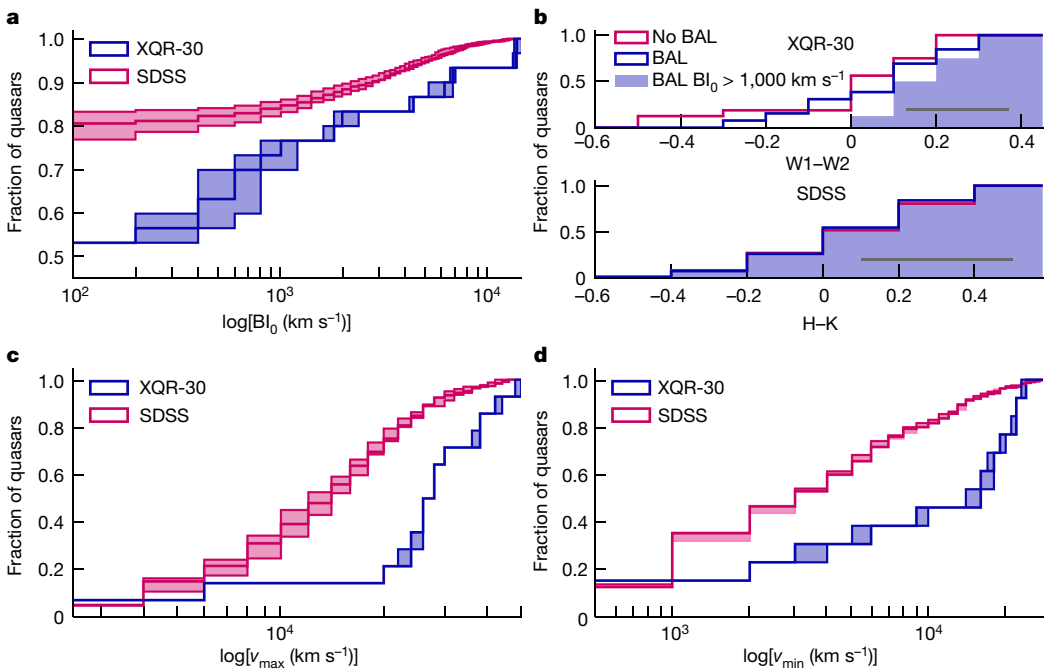

Fig. 2 | Properties of C IV BAL quasars. **a**, BI_0 cumulative distribution for the XQR-30 sample (blue solid line), compared with that of SDSS quasars at $z \simeq 2$–3. Uncertainties corresponding to a 68% confidence interval are indicated by the shaded areas. **b**, Cumulative distribution of the rest-frame optical colour, as traced by WISE (ref. [28]) W1–W2 colour for XQR-30 quasars, and the equivalent 2MASS (ref. [29]) H–K colour distribution for SDSS quasars. The error bars show the typical colour uncertainty, computed by propagating the photometry uncertainties[8]. All magnitudes are in the AB system. In total, 13 XQR-30 BAL quasars are shown, because the WISE photometry of PSOJ065+01 is contaminated by nearby sources. **c**, **d**, Maximum (**c**) and minimum (**d**) velocity cumulative distributions of the BAL outflows. Shaded areas indicate 68% confidence interval uncertainties.

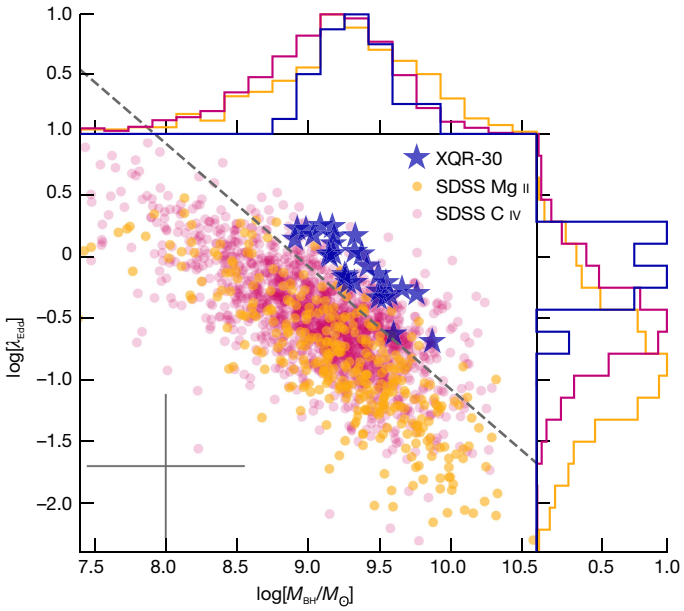

Fig. 3 | Nuclear quasar properties. The main panel shows the Eddington accretion rate (λ_{Edd}) as a function of the black-hole mass (M_{BH}). XQR-30 quasars are shown as blue stars and SDSS control sample quasars are indicated by orange and magenta circles. The error bars show the typical uncertainties, dominated by the systematics associated with single-epoch virial mass relations (Methods). The top (respectively, right) histogram shows the M_{BH} (respectively, λ_{Edd}) distributions for the two samples. M_{BH} of XQR-30 quasars and SDSS quasars with $z < 2.3$ have been derived from the Mg II line, whereas for $z > 2.3$ SDSS quasars it is based on the C IV line, correcting for non-virial motions. To build an M_{BH}- and λ_{Edd}-matched sample of SDSS quasars, sources above the dashed line in the main panel have been considered.

depend on the quasar luminosity: it is 18.9 ± 3.8% when selecting only the most luminous SDSS quasars (bolometric luminosity $L_{bol} \gtrsim 10^{47}$ erg s^{-1}), which probe the same luminosity range of our XQR-30 sample. Previous works reported no trend, or only a minor trend, of a higher BAL fraction with increasing L_{bol} in quasar samples at $z \approx 2$–4 (refs. [13,15]). Consistently, a BAL fraction of 24 ± 5% was measured in hyperluminous, infrared-selected quasars at $z \approx 2$–4.5 (ref. [16]). The SDSS BAL fraction does not increase ($19.0^{+4.3}_{-3.5}$%) when considering quasars that match the black-hole mass and accretion rate distributions of the XQR-30 sample (Fig. 3).

We find that BAL XQR-30 quasars with the most powerful outflows ($BI_0 > 1{,}000$ km s^{-1}) also show redder rest-frame optical colours than non-BAL quasars (Fig. 2), suggesting a link between the slope of the optical spectrum and the presence of strong BAL outflows at $z \gtrsim 5.8$. These BAL quasars may be dustier than non-BAL quasars. Dust may be located close to the nucleus (in the dusty torus, or in the quasar broad/narrow line region), embedded in the BAL clouds or extended on a galaxy scale, but current data do not allow us to discriminate between these scenarios. No such difference in the rest-frame optical colours of BAL and non-BAL quasars is observed in the SDSS control sample, suggesting that BAL outflows at $z \gtrsim 5.8$ may trace a peculiar phase of black-hole growth.

The maximum and minimum velocity distributions (v_{max} and v_{min}) of the C IV BAL outflows in XRQ-30 quasars are significantly different from those of the SDSS sample. Indeed, more than half of the XQR-30 BAL quasars have $v_{min} > 15{,}000$ km s^{-1}, and all but two have $v_{max} > 20{,}000$ km s^{-1}, whereas the SDSS control sample has much lower median velocities ($\langle v_{min} \rangle = 3{,}700$ km s^{-1} and $\langle v_{max} \rangle = 14{,}000$ km s^{-1}; Fig. 2). Our statistical analysis shows that the v_{max} distributions of XQR-30 and SDSS quasars are drawn from different parent populations (see Methods). Seventeen per cent of XQR-30 quasars show extremely high-velocity BAL outflows ($v_{max} > 0.1c$, with c being the speed of light), which have recently also been identified in two other $z \gtrsim 7$ quasars[1,17]. These objects are rarely observed in the total SDSS quasar population at $z \lesssim 4.5$ (ref. [18]) and are found to represent a few per cent of the brightest $z \approx 2$–4.5 quasars[16]. We conclude that BAL winds in $z \gtrsim 5.8$ quasars are significantly faster than at a lower redshift. Their extreme velocities might be explained by the presence of dust mixed with the BAL clouds, because of the higher radiation boost efficiency on dust than on the ionized gas[19,20]. Higher outflow velocities in $z \gtrsim 6$ quasars have also been suggested by studies of UV emission line blueshifts[11].

Despite the difficulty of measuring precise outflow masses at $z \approx 6$, as non-saturated absorption lines are embedded in a dense Lyman-α (Lyα) forest, we can nevertheless estimate how much energy is released in the surrounding interstellar medium by these strong winds. If the wind masses at $z \gtrsim 5.8$ are similar to those measured in lower redshift BALs[21,22], the BAL kinetic power ($\dot{E}_{kin}$) in XQR-30 quasars would be more than 10 times higher than in lower redshift BAL quasars, because of the systematically higher v_{max}. As $\dot{E}_{kin}$ of BAL winds in low-z quasars is in the range 0.001–0.03L_{bol} (ref. [23]), $\dot{E}_{kin}$ of XQR-30 BAL quasars is probably 0.01–0.3L_{bol}, which implies a huge kinetic power injected into the host galaxies. Furthermore, the higher BAL fraction at $z \gtrsim 5.8$ strongly points towards a scenario in which either the BAL wind geometry or the timescale evolves with cosmic time. The BAL fraction measured in XQR-30 quasars corresponds to a BAL divergence angle of 20–30° in the standard scenario for the BAL structure[24], and indicates that the wind blow-out phase is about half the duration of the active phase of the supermassive black hole powering the quasar. We conclude that quasars in the early Universe ($z \gtrsim 5.8$) collectively inject in their hosts ≳20 times more energy (a factor of ≈10 because of their higher velocities and a factor of ≈2.4 for the higher BAL fraction) with respect to quasars at $z \approx 2$–3. This energy injection can probably inhibit further gas accretion, slowing down black-hole growth.

At the same time, the host galaxies of high-redshift quasars are growing rapidly, with star-formation rates (SFRs) that typically reach thousands of solar masses ($M_{\odot}$) per year (refs. [25,26]). Therefore, high-z BAL quasars may be witnessing the onset of substantial black-hole feedback and marking the transition from a growth phase in which black-hole growth is dominant to a phase of black-hole and host-galaxy symbiotic growth[3]. Cosmological, hydrodynamic simulations of early black-hole and galaxy evolution support this scenario by identifying $z \approx 6$–7 as the transition epoch during which quasar feedback increases in strength and starts to markedly slow down black-hole growth[4,27].

Atacama Large Millimetre/submillimetre Array and, in perspective, James Webb Space Telescope observations of XQR-30 BAL quasars will be fundamental to compare dust and SFR properties with those of non-BAL quasars. A difference in the dust properties will favour a scenario of BAL quasars being caught in a peculiar evolutionary phase, whereas no distinction will imply a redshift evolution in terms of the BAL outflow geometry. Finally, a measure of the SFR will allow us to determine whether $z \gtrsim 6$ BAL quasars are experiencing a different growth phase from that experienced by non-BAL quasars and whether BAL quasars can be used as tracers of ongoing black-hole feedback at these early epochs.

Online content

Any methods, additional references, Nature Research reporting summaries, source data, extended data, supplementary information, acknowledgements, peer review information; details of author contributions and competing interests; and statements of data and code availability are available at https://doi.org/10.1038/s41586-022-04608-1.

1. Wang, F. et al. A luminous quasar at redshift 7.642. *Astrophys. J. Lett.* **907**, L1 (2021).
2. Neeleman, M. et al. The kinematics of $z \gtrsim 6$ quasar host galaxies. *Astrophys. J.* **911**, 141 (2021).

3. Volonteri, M. The formation and evolution of massive black holes. *Science* **337**, 544–547 (2012).
4. Van der Vlugt, D. & Costa, T. How AGN feedback drives the size growth of the first quasars. *Mon. Not. R. Astron. Soc.* **490**, 4918–4934 (2019).
5. Hickox, R. C. & Alexander, D. M. Obscured active galactic nuclei. *Annu. Rev. Astron. Astrophys.* **56**, 625 (2018).
6. Weymann, R. J., Morris, S. L., Foltz, C. B. & Hewett, P. C. Comparisons of the emission-line and continuum properties of broad absorption line and normal quasi-stellar objects. *Astrophys. J.* **373**, 23–53 (1991).
7. Gibson, R. R. et al. A catalog of broad absorption line quasars in Sloan Digital Sky Survey Data Release 5. *Astrophys. J.* **692**, 758–777 (2009).
8. Shen, Y. et al. A catalog of quasar properties from Sloan Digital Sky Survey Data Release 7. *Astrophys. J. Suppl. Ser.* **194**, 45 (2011).
9. Cameron, E. On the estimation of confidence intervals for binomial population proportions in astronomy: the simplicity and superiority of the Bayesian approach. *Publ. Astron. Soc. Aust.* **28**, 128–139 (2011).
10. Shen, Y. et al. Gemini GNIRS near-infrared spectroscopy of 50 quasars at $z \gtrsim 5.7$. *Astrophys. J.* **873**, 35 (2019).
11. Schindler, J.-T. et al. The X-shooter/ALMA sample of quasars in the epoch of reionization. I. NIR spectral modeling, iron enrichment, and broad emission line properties. *Astrophys. J.* **905**, 51 (2020).
12. Yang, J. et al. Probing early super-massive black hole growth and quasar evolution with near-infrared spectroscopy of 37 reionization-era quasars at $6.3 < z \leq 7.64$. *Astrophys. J.* **923**, 262 (2021).
13. Allen, J. T., Hewett, P. C., Maddox, N., Richards, G. T. & Belokurov, V. A strong redshift dependence of the broad absorption line quasar fraction. *Mon. Not. R. Astron. Soc.* **410**, 860–884 (2011).
14. Trump, J. R. et al. A catalog of broad absorption line quasars from the Sloan Digital Sky Survey Third Data Release. *Astrophys. J. Suppl. Ser.* **165**, 1–18 (2006).
15. Dai, X., Shankar, F. & Sivakoff, G. R. 2MASS reveals a large intrinsic fraction of BALQSOs. *Astrophys. J.* **672**, 108–114 (2008).
16. Bruni, G. et al. The WISSH quasars project. VI. Fraction and properties of BAL quasars in the hyper-luminosity regime. *Astron. Astrophys.* **630**, A111 (2019).
17. Wang, F. et al. The discovery of a luminous broad absorption line quasar at a redshift of 7.02. *Astrophys. J. Lett.* **869**, L9 (2018).
18. Rodríguez Hidalgo, P. et al. Survey of extremely high-velocity outflows in Sloan Digital Sky Survey quasars. *Astrophys. J.* **896**, 151 (2021).
19. Ishibashi, W., Banerji, M. & Fabian, A. C. AGN radiative feedback in dusty quasar populations. *Mon. Not. R. Astron. Soc.* **469**, 1496–1501 (2017).
20. Costa, T., Rosdahl, J., Sijacki, D. & Haehnelt, M. G. Driving gas shells with radiation pressure on dust in radiation-hydrodynamic simulations. *Mon. Not. R. Astron. Soc.* **473**, 4197–4219 (2018).
21. Dunn, J. P., Crenshaw, D. M., Kraemer, S. B. & Trippe, M. L. Physical conditions in the ultraviolet absorbers of IRAS F22456-5125. *Astrophys. J.* **713**, 900–905 (2010).
22. Moe, M., Arav, N., Bautista, M. A. & Korista, K. T. Quasar outflow contribution to AGN feedback: observations of QSO SDSS J0838+2955. *Astrophys. J.* **706**, 525–534 (2009).
23. Fiore, F. et al. AGN wind scaling relations and the co-evolution of black holes and galaxies. *Astron. Astrophys.* **601**, A143 (2017).
24. Elvis, M. A structure for quasar. *Astrophys. J.* **545**, 63–76 (2000).
25. Decarli, R. et al. An ALMA [C II] survey of 27 quasars at $z > 5.94$. *Astrophys. J.* **854**, 97 (2018).
26. Eilers, A.-C. et al. Detecting and characterizing young quasars. I. Systemic redshifts and proximity zone measurements. *Astrophys. J.* **900**, 37 (2020).
27. Costa, T., Sijacki, D., Trenti, M. & Haehnelt, M. G. The environment of bright QSOs at $z \sim 6$: star-forming galaxies and X-ray emission. *Mon. Not. R. Astron. Soc.* **439**, 2146–2174 (2014).
28. Wright, E. L. et al. The Wide-field Infrared Survey Explorer (WISE): mission description and initial on-orbit performance. *Astron. J.* **140**, 1868–1881 (2010).
29. Skrutskie, M. F. et al. The Two Micron All Sky Survey (2MASS). *Astron. J.* **131**, 1163–1183 (2006).

Methods

XQR-30 sample and X-shooter observations

XQR-30 quasars were selected to match the following requirements: declination $\delta < +27°$, to be observable from the European Southern Observatory (ESO)/Very Large Telescope; redshift $z \geq 5.8$, to require the Mg II emission line in the K band; J magnitude $J_{AB} \leq 19.8$ for $z < 6.0$ sources and $J_{AB} \leq 20.0$ for quasars at $z \geq 6.0$; no existing deep X-shooter data, defined as $S/N \gtrsim 25$ per 50 km s^{-1} pixel at 1,600–1,700 Å. The application of those constraints to the literature[30,31] and newly discovered quasars resulted in a sample of 30 sources covering the redshift range $5.8 \leq z \leq 6.6$ (Extended Data Table 1). The X-shooter spectra have been acquired with slit widths of 0.9 arcsec and 0.6 arcsec, and resolving power of $R \approx 8{,}900$ and 8,100, in the visible (Vis) and NIR arms, respectively. The observing time on target ranges from 4 h to 11 h. The median S/N ratio per pixel in the rest-frame 1,600–1,700 Å wavelength range is between 25 and 160 for spectra rebinned to 50 km s^{-1}, as used in this work. Raw frames have been reduced with a custom software pipeline developed in the collaboration[32]. A relative flux calibration has been applied to all reduced spectra by considering the instrument response curve built from a single spectrophotometric standard star for all frames. A comparison between the spectra obtained by this method with those reduced with the ESO pipeline[33] and calibrated with standard stars acquired on the same night of the observation does not show significant differences. X-shooter Vis and NIR spectra have been combined with the Astrocook software[34] by scaling the NIR to the Vis using the median values computed in the overlapping spectral region 10,000–10,200 Å (in the observed frame). We checked that this procedure had not introduced any spectral artefact in the X-shooter data by visual inspection of all XQR-30 spectra. We note that the ≈10,000 Å spectral region (magenta area in Fig. 3, and Extended Data Figs. 1 and 2) can be spuriously affected by an anomalous drop in the X-shooter response curve of the Vis arm. If this effect is not properly corrected, it may result in a flux drop in the X-shooter spectrum mimicking weak BAL absorption between C IV and Si IV for a $z \approx 6.0$ quasar. We have verified that this effect does not evidently affect BAL quasars in XQR-30 because no significant variation in the normalization of the Vis spectrum around 10,000 Å is observed between different exposures. Nevertheless, as a minor flux drop not detectable in the individual exposures might still be present, we also report the BAL fraction in XQR-30 after excluding the three weak BAL quasars (namely J0408-5632, SDSSJ0842+1218 and SDSSJ2310+1855) in which the absorption falls in the overlap region. The absolute flux calibration has been obtained by normalizing the combined spectrum to the J-band photometry[30,35–40].

Imaging observations

Four of the quasars in the sample had no published J-band information in the literature, and we present their J-band AB magnitudes in Extended Data Table 1, namely ATLASJ029-36, PSOJ065+01, PSOJ065-26 and J2211-3206. For J2211-3206, we report the magnitude from the VIKING DR4 catalogue[41]. We observed ATLASJ029-35 and PSOJ065-26 on 24 September 2017 for 6 min each with the Fourstar infrared camera[42] at the Magellan Baade 6.5-m telescope at Las Campanas observatory. PSOJ065+01 was observed on 21 December 2018 for 5 min with the SofI camera[43] mounted on the New Technology Telescope at La Silla observatory. The images were processed with standard reduction steps (bias subtraction, flat fielding, sky subtraction, stacking) and the photometry was calibrated against stellar sources in the 2MASS catalogue.

Selection/completeness effects and SDSS control samples

The observed BAL fraction is the result of an intrinsic BAL quasar distribution convolved with quasar selection criteria. Using standard quasar colour selection could result in missing several BAL quasars because their UV colours, affected by the absorption troughs, may resemble that of stars, leading to their exclusion from spectroscopic samples. Several authors tried to estimate intrinsic BAL fractions by computing correction factors as a function of redshift. The uncertainty on these correction factors is however quite large, at least a factor of a few, even considering the same set of selection/completeness effects and similar redshift intervals[7,13,44,45]. In fact, the intrinsic BAL fraction strongly depends on the input BAL properties, such as the intrinsic distribution of BAL velocity, depth, and their relation with reddening, which are all basically unknown. The spread of plausible assumptions naturally leads to large uncertainties. On the other hand, selection effects could be minimized, and made significantly smaller than the uncertainty in estimating intrinsic BAL fractions, by using quasar samples selected in the rest-frame optical, avoiding the biases generated by UV absorption troughs in the colour selection. In these cases, the observed-to-intrinsic BAL fraction correction is known to be modest, less than 10–20% (refs. [15,46]). The fact that most BAL quasars are recovered with a rest-frame optical selection is supported by the fact that any other quasar selection (from X-ray to radio wavelengths) generally results in a lower or similar BAL fraction to that measured in rest-frame optically selected quasars[47–49]. Therefore, we choose to compare the observed XQR-30 BAL fraction with those observed in quasar samples at different redshifts with selection criteria matched to the XQR-30 sample.

Although the XQR-30 quasars have been discovered through rest-frame UV colours probing the Lyα break, an extra WISE (ref. [28]) W1–W2 (3.4–4.6 μm) colour (rest-frame optical) was used to discriminate between $z \gtrsim 6$ quasar candidates and stars in the photometric searches[30,39,50,51]. Starting from a catalogue of SDSS DR7 quasars[8], we selected the 11,800 quasars in the redshift range $2.13 < z < 3.20$ for which the 1,216–2,100 Å wavelength range is covered by SDSS spectroscopy and the H (1.7 μm) and K (2.2 μm) bands probe similar rest-frame spectral regions covered by W1 and W2 bands for the XQR-30 quasars. We require the control sample to be detected by the 2MASS survey[29] in both the H and K bands. We exclude noisy spectra by requiring a median $S/N > 5$ in the 1,500–1,600 Å range. The resulting sample consists of 1,580 quasars (BAL fraction $19.4^{+1.3}_{-1.1}$%, $BI_0 > 100$ km s^{-1}). We also study two subsamples of the first control sample, one with $L_{bol} \gtrsim 10^{47}$ erg s^{-1} and $2.13 < z < 3.20$, probing the same luminosity range of the XQR-30 sample (275 quasars, BAL fraction 18.9 ± 3.8%). The same BAL fraction is recovered when requiring a match in absolute magnitude $M_{1,450Å}$. The second of the two subsamples has high $\lambda_{Edd} = L_{bol}/L_{Edd}$ (in which L_{Edd} is the Eddington luminosity) and $2.13 < z < 3.20$, including 268 quasars above the black dashed line in Fig. 3, matching M_{BH} and λ_{Edd} distributions of XQR-30 quasars (BAL fraction $19.0^{+4.3}_{-3.5}$%).

The redshift interval $2.13 < z < 3.20$ contains subranges in which the completeness of the SDSS quasar selection algorithm is low. As a different completeness for BAL and non-BAL quasars may bias the measured BAL fraction, we consider the range of estimates from the literature[13,44] to select those intervals in which this difference is relatively modest: $2.13 < z < 2.2$, including 263 quasars, for which we measure a BAL fraction of $17.5^{+4.2}_{-3.5}$%, close to that found for the first complete SDSS control sample. As a further check, we consider a further sample of 313 SDSS DR7 quasars in the redshift range 3.6–4.6, where the completeness is more than 90% for both BAL and non-BAL quasars (as for the first quasar control sample, we selected only quasars with a K-band detection). At these redshifts, SDSS spectroscopy covers the 1,216–1,640 Å wavelength range. The BAL fraction is $19.2^{+3.8}_{-3.4}$, again very similar to the fraction found for the first SDSS control sample. We conclude that selection completeness does not significantly affect the BAL fraction measured using equation (1). Therefore, throughout this study we compare the results on the XQR-30 sample with those of the first complete SDSS control sample.

BAL identification

To search for BAL absorption troughs, it is necessary to model the intrinsic quasar continuum emission. A common approach consists

of fitting the observed spectra with a continuum model[7]. This however requires a sufficiently large portion of the spectral band to be free from absorption or emission features, a condition usually not met in quasar spectra bluewards of C IV. We thus adopt a different method to estimate the quasar continuum for the XQR-30 sample. We create composite emission templates based on the catalogue of 11,800 quasars at $2.13 \lesssim z \lesssim 3.20$ from SDSS DR7 as defined above. For each XQR-30 spectrum, the template is the median of 100 non-BAL[7] quasar spectra, randomly selected from SDSS in the redshift range $2.13 \lesssim z \lesssim 3.20$ (to cover the 1216–2,100 Å rest wavelength range), with colours and C IV equivalent width in a range encompassing ±20% the values measured for the XQR-30 quasar. For the quasar colours we consider the F(1,700 Å)/F(2,100Å) and F(1,290 Å)/F(1,700 Å) flux ratios, F(1,700 Å) and F(2,100 Å) being median values over 100 Å and F(1,290 Å) being a median value over 30 Å in the rest frame. We assume that observed and intrinsic continuum emission do not differ at ≈1,290 Å (except in the case of PSOJ065+01, for which we anchored the fit to the emission at 1,330–1,350 Å), the bluest spectral region in which continuum emission can be probed in the XQR-30 spectra, owing to the strong Lyα forest absorption at $\lambda \lesssim 1{,}216$ Å. This may represent a lower limit to the intrinsic quasar emission in the case that BAL absorption troughs affect the ≈1,290 Å spectral region. For XQR-30 sources with redder colours (that is, F(1,700 Å)/F(2,100 Å) $\lesssim 1$ and F(1,290 Å)/F(1,700 Å) < 1), the composite spectrum is built from 30–60 SDSS quasars that match our criteria, owing to the relative rarity of red quasars in SDSS. The combined template has a spectral resolution of ≈70 km s^{-1} in the C IV spectral region, which corresponds to the lower spectral resolution of the individual SDSS spectra, and is normalized to the median value of the XQR-30 quasar spectrum in the 1,650–1,750 Å interval. The last of these has been chosen as it is free from prominent emission lines and strong telluric absorption in the X-shooter spectra. The normalized XQR-30 spectra are then obtained by dividing each X-shooter spectrum by the matched composite SDSS template. We measure the BI_0 (ref. [6]) according to the following definition[7]:

$$BI_0 = \int_0^{v_{lim}} \left(1 - \frac{f(v)}{0.9}\right) C dv \quad (1)$$

in which $f(v)$ is the normalized spectrum, $C = 1$ if $f(v) < 0.9$ for contiguous troughs of >2,000 km s^{-1}, and $C = 0$ otherwise. The uncertainties on BI_0, dominated by the accuracy of the composite template, allow us to measure with high reliability $BI_0 \gtrsim 100$ km s^{-1} in our XQR-30 spectra and in the SDSS control samples. We identify the minimum v_{min} and maximum v_{max} BAL velocity for a given transition as the lowest and highest velocity for which $C = 1$ in equation (1), respectively. Our approach differs from most identification studies of BAL quasars in SDSS, which typically adopt $v_{lim} = 25{,}000$ km s^{-1} (refs. [7,52]). The latter choice accounts only for BAL features in the spectral region between C IV and Si IV and, therefore, underestimates BI_0 for BAL systems with $v_{max} > 25{,}000$ km s^{-1}, and completely misses BAL systems with $v_{min} > 25{,}000$ km s^{-1}. Our analysis is limited to $v_{lim} < 64{,}500$ km s^{-1} with respect to C IV, because in $z \approx 6$ quasar spectra almost no transmitted flux is observed bluewards of the Lyα emission. Given that the C IV optical depth usually dominates the Si IV depth in BAL quasars[53], we use the velocity range of the C IV BAL troughs to identify absorption associated with Si IV (ref. [17]). This implies that broad absorption features bluewards of Si IV are ascribed to a low-velocity Si IV BAL if a C IV BAL with similar velocity is observed in the X-shooter spectrum. This is the case for XQR-30 quasars J0923+0402, PSOJ089-015, VDESJ2211-3206, PSOJ239-07 and PSOJ023-02. Otherwise, broad absorption features bluewards of Si IV are due to a high-velocity ($v_{max} \gtrsim 30{,}000$ km s^{-1}) C IV BAL. We use the same methodology to identify N V BAL features. Among the 14 C IV BAL quasars identified (Extended Data Table 1), 8 show also a Si IV BAL, 3 a N V BAL and 1 a Mg II BAL. Quasars J0923+0402, PSOJ089-15, VDESJ2211-3206 and PSOJ231-20 had been already classified as BAL by visual inspection[11,26,31,54]. The characterization of non-C IV BAL outflows will be presented elsewhere (M.B. et al., manuscript in preparation).

Uncertainties on the BAL parameters in XQR-30 quasars are estimated by taking into account the uncertainty on the composite template slope (we create a 'bluer' and a 'redder' template considering the 33% bluest and the 33% reddest spectra among those contributing to the best-fit template, respectively) and the uncertainty on the composite template normalization (we increase (respectively, lower) the flux of the bluer (respectively, redder) template by a factor of σ_{stat}, with σ_{stat} being the median noise of the X-shooter spectrum in the range 1,650–1,750 Å). We verified that the resulting uncertainties correspond to a 68% confidence interval. The bluer and redder templates are used to create new normalized XQR-30 spectra, from which the range of variation of BI_0, v_{min} and v_{max} is measured. The same approach is used to calculate the uncertainties on the BAL properties for the SDSS control sample.

Statistical tests

To calculate the probability that the BAL fraction in XQR-30 traces the same BAL quasar population of SDSS $z \approx 2$–3 quasars, we generated 10^6 subsamples of 30 randomly selected, non-repeated quasars from the SDSS comparison sample, and computed the probability to observe ≥14 BALs out of 30 quasars as $p_{rand}(BI_0) = N_{\geq 14}/10^6$, in which $N_{\geq 14}$ is the number of subsamples with ≥14 BAL quasars. This probability is 2×10^{-4}. A Mann–Whitney U-test[55] rejects the hypothesis that the BI_0 distributions of XQR-30 and the SDSS control sample are equal with probability $p_U(BI_0) = 2.6 \times 10^{-4}$. If we exclude the three quasars whose BAL absorption falls close to the edge of the X-shooter Vis arm, we obtain $p_{rand}(BI_0) = N_{\geq 11}/10^6 = 3.3 \times 10^{-3}$ and $p_U(BI_0) = 2.8 \times 10^{-3}$. The randomly generated subsamples of SDSS quasars have been similarly used to calculate the probability of observing by chance in the SDSS control sample 57% of the BAL quasars with $v_{min} > 15{,}000$ km s^{-1} and 86% of the BAL quasars with $v_{max} > 20{,}000$ km s^{-1}. These probabilities are $p_{rand}(v_{min}) = 4 \times 10^{-5}$ and $p_{rand}(v_{max}) < 10^{-6}$. The U-test for the hypothesis that the v_{max} distributions for the XQR-30 and SDSS control samples are drawn from the same parent population gives a probability $p_U(v_{max}) = 8 \times 10^{-5}$.

Nuclear properties

The black-hole mass and accretion rate for the XQR-30 sample have been derived by spectral modelling of the Mg II spectral region in the X-shooter data, by taking into account the quasar power-law continuum and the Balmer pseudo-continuum emission[13,39], the Fe II emission[56] and one or more Gaussian components to model the Mg II emission line profile. Details of the spectral analysis, as well as the individual M_{BH} and λ_{Edd}, will be presented elsewhere (C.M. et al., manuscript in preparation). We calculate $\lambda_{Edd} = L_{bol}/L_{Edd}$, in which L_{bol} is derived from the monochromatic luminosity at 3,000 Å through bolometric correction[57,58]; M_{BH} is based on the total full-width at half-maximum of the Mg II line profile[39]. The same method has been applied to the SDSS control sample quasars with Mg II measurements[8] ($z \lesssim 2.3$). In particular, the same Fe II modelling and single-epoch relation[59] have been used. For the remaining SDSS quasars ($z > 2.3$), M_{BH} and λ_{Edd} are based on the C IV line[8,60]. We correct for the presence of non-virial motions affecting the C IV profile[61].

Data availability

X-shooter raw data used in this work are publicly available on the ESO Science Archive (http://archive.eso.org/cms.html). Reduced data are available upon request at the date of writing and will be released by the XQR-30 collaboration once observations are completed.

30. Bañados, E. et al. The Pan-STARRS1 Distant z > 5.6 Quasar Survey: more than 100 quasars within the first Gyr of the Universe. *Astrophys. J. Suppl. Ser.* **227**, 11 (2016).
31. Wang, F. et al. Exploring reionization-era quasars. III. Discovery of 16 quasars at $6.4 \lesssim z \lesssim 6.9$ with DESI Legacy Imaging Surveys and the UKIRT Hemisphere Survey and quasar luminosity function at $z \sim 6.7$. *Astrophys. J. Lett.* **884**, 30 (2019).

32. López, S. et al. XQ-100: a legacy survey of one hundred $3.5 \lesssim z \lesssim 4.5$ quasars observed with VLT/X-shooter. *Astron. Astrophys.* **594**, A91 (2016).
33. Modigliani, A. et al. In *Soc. Photo-Opt. Instr. Eng. Conf. Ser. Observatory Operations: Strategies, Processes, and Systems III* Vol. 7737 (eds Silva, D. R. et al.) 773728 (SPIE, 2010).
34. Cupani, G. et al. In *Soc. Photo-Opt. Instr. Eng. Conf. Series* Vol. 11452, 114521U (SPIE, 2020).
35. Ross, N. P. & Cross, N. J. G. The near and mid-infrared photometric properties of known redshift $z \gtrsim 5$ quasars. *Mon. Not. R. Astron. Soc.* **494**, 789–803 (2020).
36. Jiang, L. et al. Discovery of eight $z \sim 6$ quasars in the Sloan Digital Sky Survey overlap regions. *Astron. J.* **149**, 188 (2015).
37. Lawrence, A. et al. The UKIRT Infrared Deep Sky Survey (UKIDSS). *Mon. Not. R. Astron. Soc.* **379**, 1599–1617 (2007).
38. Cross, N. J. G. et al. The VISTA Science Archive. *Astron. Astrophys.* **548**, A119 (2012).
39. Mazzucchelli, C. et al. Physical properties of 15 quasars at $z \gtrsim 6.5$. *Astrophys. J.* **849**, 91 (2017).
40. Bañados, E. et al. A metal-poor damped Lyα system at redshift 6.4. *Astrophys. J.* **885**, 59 (2019).
41. Edge, A. et al. The VISTA Kilo-degree Infrared Galaxy (VIKING) Survey: bridging the gap between low and high redshift. *Messenger* **154**, 32–34 (2013).
42. Persson, S. E. et al. FourStar: the near-infrared imager for the 6.5 m Baade Telescope at Las Campanas Observatory. *Publ. Astron. Soc. Pac.* **125**, 654–682 (2013).
43. Moorwood, A., Cuby, J. G. & Lidman, C. SOFI sees first light at the NTT. *Messenger* **91**, 9–13 (1998).
44. Reichard, T. A. et al. Continuum and emission-line properties of broad absorption line quasars. *Astron. J.* **126**, 2594–2607 (2003).
45. Knigge, C., Scaringi, S., Goad, M. R. & Cottis, C. E. The intrinsic fraction of broad-absorption line quasars. *Mon. Not. R. Astron. Soc.* **386**, 1426–1435 (2008).
46. Maddox, N., Hewett, P. C., Warren, S. J. & Croom, S. M. Luminous K-band selected quasars from UKIDSS. *Mon. Not. R. Astron. Soc.* **386**, 1605–1624 (2008).
47. Giustini, M., Cappi, M. & Vignali, C. On the absorption of X-ray bright broad absorption line quasars. *Astron. Astrophys.* **491**, 425–434 (2008).
48. White, R. L. et al. An I-band-selected sample of radio-emitting quasars: evidence for a large population of red quasars. *Astron. J.* **126**, 706–722 (2003).
49. Becker, R. H. et al. Properties of radio-selected broad absorption line quasars from the first bright quasar survey. *Astrophys. J.* **538**, 72–82 (2000).
50. Chehade, B. et al. Two more, bright, $z > 6$ quasars from VST ATLAS and WISE. *Mon. Not. R. Astron. Soc.* **478**, 1649–1659 (2018).
51. Reed, S. L. et al. Eight new luminous $z \geq 6$ quasars discovered via SED model fitting of VISTA, WISE and Dark Energy Survey Year 1 observations. *Mon. Not. R. Astron. Soc.* **468**, 4702–4718 (2017).
52. Pâris, I. et al. The Sloan Digital Sky Survey Quasar Catalog: fourteenth data release. *Astron. Astrophys.* **613**, A51 (2018).
53. Dunn, J. P. et al. BAL outflow contribution to AGN feedback: frequency of S IV outflows in the SDSS. *Astrophys. J.* **750**, 143 (2012).
54. Connor, T. et al. X-ray observations of a [C II]-bright, $z = 6.59$ quasar/companion system. *Astrophys. J.* **900**, 189 (2020).
55. Mann, H. B. & Whitney, D. R. On a test of whether one of two random variables is stochastically larger than the other. *Ann. Math. Stat.* **18**, 50–60 (1947).
56. Vestergaard, M. & Wilkes, B. An empirical ultraviolet template for iron emission in quasars as derived from I Zwicky 1. *Astrophys. J. Supp.* **134**, 1–33 (2001).
57. Runnoe, J. C., Brotherton, M. S. & Shang, Z. Updating quasar bolometric luminosity corrections. *Mon. Not. R. Astron. Soc.* **422**, 478–493 (2012).
58. Runnoe, J. C., Brotherton, M. S. & Shang, Z. Erratum: Updating quasar bolometric luminosity corrections. *Mon. Not. R. Astron. Soc.* **427**, 1800 (2012).
59. Vestergaard, M. & Osmer, P. S. Mass functions of the active black holes in distant quasars from the large bright quasar survey, the bright quasar survey, and the color-selected sample of the SDSS fall equatorial stripe. *Astrophys. J.* **699**, 800–816 (2009).
60. Vestergaard, M. & Peterson, B. M. Determining central black hole masses in distant active galaxies and quasars. II. Improved optical and UV scaling relationships. *Astrophys. J.* **641**, 689–709 (2006).
61. Coatman, L. et al. Correcting C IV-based virial black hole masses. *Mon. Not. R. Astron. Soc.* **465**, 2120–2142 (2017).

Acknowledgements This work is based on observations collected at the European Organisation for Astronomical Research in the Southern Hemisphere under ESO large programme 1104.A-0026(A) and ESO programme 0102.A-0233(A). Funding for SDSS and SDSS-II has been provided by the Alfred P. Sloan Foundation, the Participating Institutions, the National Science Foundation, the US Department of Energy, the National Aeronautics and Space Administration, the Japanese Monbukagakusho, the Max Planck Society and the Higher Education Funding Council for England. The SDSS website is http://www.sdss.org/. The SDSS is managed by the Astrophysical Research Consortium for the Participating Institutions. The Participating Institutions are the American Museum of Natural History, the Astrophysical Institute Potsdam, the University of Basel, the University of Cambridge, Case Western Reserve University, the University of Chicago, Drexel University, Fermilab, the Institute for Advanced Study, the Japan Participation Group, Johns Hopkins University, the Joint Institute for Nuclear Astrophysics, the Kavli Institute for Particle Astrophysics and Cosmology, the Korean Scientist Group, the Chinese Academy of Sciences (LAMOST), Los Alamos National Laboratory, the Max-Planck-Institute for Astronomy, the Max-Planck-Institute for Astrophysics, New Mexico State University, Ohio State University, the University of Pittsburgh, the University of Portsmouth, Princeton University, the United States Naval Observatory, and the University of Washington. M.B., C.F., F.F. and E.P. acknowledge support from the PRIN MIUR project 'Black hole winds and the baryon life cycle of galaxies: the stone-guest at the galaxy evolution supper', contract number 2017PH3WAT. R.D. is supported by a Gruber Foundation Fellowship grant. G.B. was supported by NSF grant AST-1751404. S.E.I.B. and R.A.M. acknowledge funding from the European Research Council under the European Union's Horizon 2020 research and innovation programme (grant agreement number 740246 'Cosmic gas'. R.M. acknowledges support by the Science and Technology Facilities Council and European Research Council Advanced Grant 695671 'QUENCH'. R.M. also acknowledges funding from a research professorship from the Royal Society. A.C.E. acknowledges support by NASA through the NASA Hubble Fellowship grant number HF2-51434 awarded by the Space Telescope Science Institute, which is operated by the Association of Universities for Research in Astronomy, Inc., for NASA, under contract NAS5-26555. This research was conducted by the Australian Research Council Centre of Excellence for All Sky Astrophysics in 3 Dimensions (ASTRO 3D), through project number CE170100013. This paper includes data gathered with the 6.5-m Magellan Telescopes located at Las Campanas Observatory, Chile.

Author contributions M.B. led the analysis and writing presented in this paper. V.D'O. is the principal investigator of the ESO/Very Large Telescope X-shooter large programme that led to our findings and contributed to the data analysis. V.D'O., C.F. and F.F. had a central role in project design and implementation. N.A. provided expertise in the topic of BAL identification and analysis methodology. E.B. provided new photometric points based on ESO observations. G.B. and G.C. carried out the reduction of the spectra. All authors are part of the XQR-30 collaboration and have reviewed, discussed and commented on the manuscript.

Additional information

Correspondence and requests for materials should be addressed to M. Bischetti.

Peer review information *Nature* thanks the anonymous reviewer(s) for their contribution to the peer review of this work.

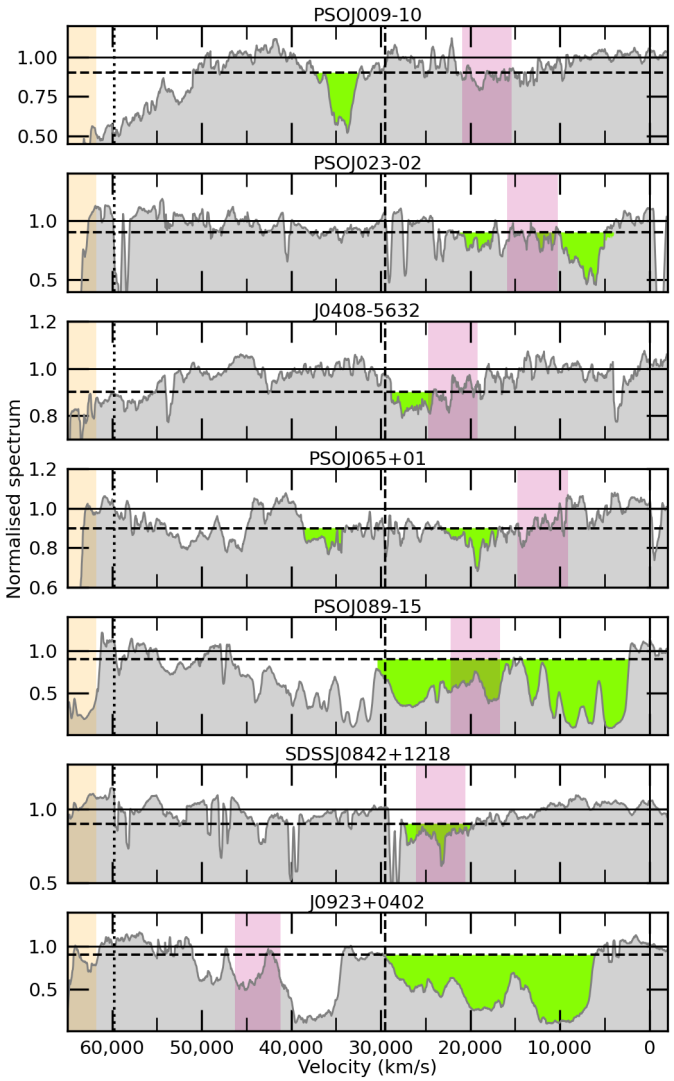

Extended Data Fig. 1 | Normalized spectra of BAL quasars in the XQR-30 sample, smoothed to 500 km/s. The velocity axis in each panel is relative to the rest-frame wavelength of C IV. Vertical solid, dashed, and dotted lines indicate the position of C IV, Si IV and N V, respectively. The horizontal solid (dashed) line represents a flux level of 1.0(0.9). C IV BALs, corresponding to a flux level of less than 0.9 (equation 1), are highlighted as green shaded areas. We note that the C IV optical depth typically dominates that of Si IV in BAL quasars. This implies that, for example, the BAL feature at v-45000 km/s in PSOJ009-10 cannot be ascribed to a low velocity Si IV BAL because no low velocity C IV BAL with similar velocity is observed in the X-shooter spectrum. The shaded magenta areas indicate the overlapping spectral region between the X-shooter Vis and NIR arms, while orange areas indicate the spectral region affected by substantial intergalactic medium absorption.

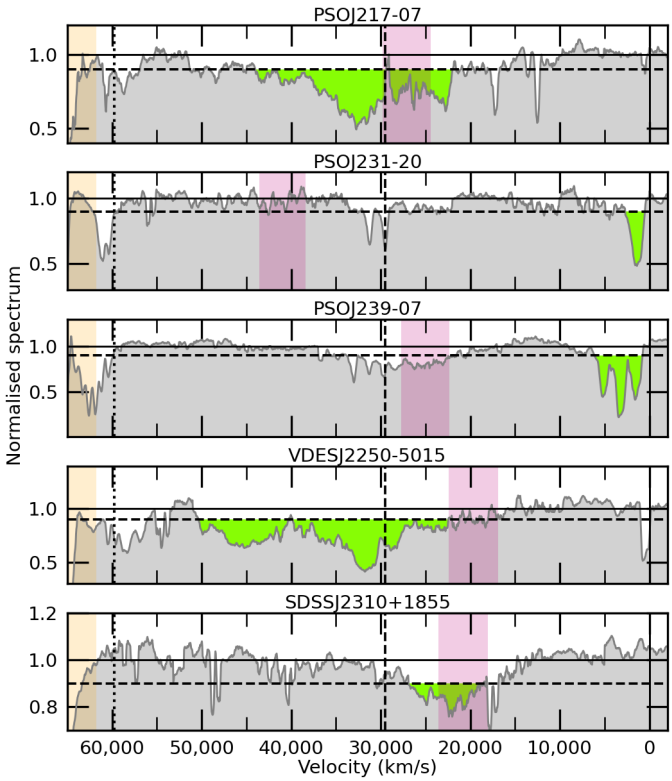

Extended Data Fig. 2 | Normalized spectra of BAL quasars in the XQR-30 sample, smoothed to 500 km/s. Same as Extended Data Figure 1.

Extended Data Table 1 | The XQR-30 sample properties and BAL system parameters

Name	Ra	Dec	SNR	$z_{\rm MgII}$	J	W1	W2	BI_0	$v_{\rm min}$	$v_{\rm max}$	Type	Ref
(1)	(2)	(3)	(4)	(5)	(6)	(7)	(8)	(9)	(10)	(11)	(12)	(13)
PSOJ007+04	00:28:06.56	+04:57:25.64	79	5.954	19.77	19.97	19.75	-	-	-	no-BAL	22,22
PSOJ009-10	00:38:56.52	-10 25 53.90	27	5.938	19.93	19.16	19.00	$1{,}110^{+130}_{-270}$	$33{,}040^{+220}_{-100}$	$38{,}380^{+150}_{-1{,}360}$	BAL	22,39
PSOJ023-02	01:32:01.70	-02:16:03.11	28	5.816	19.78	19.20	18.82	$2{,}120^{+370}_{-180}$	$3{,}950^{+150}_{-370}$	$21{,}240^{+690}_{-90}$	BAL	22,22
PSOJ025-11	01:40:57.03	-11:40:59.48	32	5.816	19.65	19.37	19.26	-	-	-	no-BAL	22,22
PSOJ029-29	01:58:04.14	-29:05:19.25	29	5.976	19.07	18.81	18.58	-	-	-	no-BAL	22,22
ATLASJ029-36	01:59:57.97	-36:33:56.60	30	6.013	19.57	19.28	19.19	-	-	-	no-BAL	(*),39
VDESJ0224-4711	02:24:26.54	-47:11:29.40	38	6.525	19.73	18.78	18.70	-	-	-	no-BAL	39,39
PSOJ060+24	04:02:12.69	+24:51:24.42	34	6.170	19.71	19.17	19.41	-	-	-	no-BAL	22,22
J0408-5632	04:08:19.23	-56:32:28.80	106	6.033	19.85	20.04	19.85	360^{+160}_{-100}	$24{,}130^{+100}_{-1{,}010}$	$28{,}820^{+170}_{-130}$	BAL	39,39
PSOJ065-26	04:21:38.05	-26:57:15.60	135	6.179	19.36	19.01	19.00	-	-	-	no-BAL	(*),22
PSOJ065+01	04:23:50.15	+01:43:24.79	25	5.804	19.74	-	-	920^{+360}_{-150}	$16{,}890^{+1{,}740}_{-1{,}980}$	$38{,}610^{+220}_{-140}$	BAL	(*)
PSOJ089-15	05:59:45.47	-15:35:00.20	102	5.972	19.17	18.18	17.80	$13{,}910^{+800}_{-680}$	$2{,}250^{+150}_{-90}$	$30{,}360^{+840}_{-160}$	BAL	22,39
PSOJ108+08	07:13:46.31	+08:55:32.65	126	5.955	19.07	18.69	18.51	-	-	-	no-BAL	39,22
SDSSJ0842+1218	08:42:29.43	+12:18: 50.58	133	6.067	19.78	19.00	19.03	740^{+150}_{-220}	$19{,}920^{+510}_{-150}$	$27{,}380^{+140}_{-90}$	BAL	40,39
J0923+0402	09:23:47.12	+04:02:54.40	30	6.626	20.28	19.20	19.05	$13{,}670^{+260}_{-170}$	$6{,}090^{+150}_{-150}$	$29{,}550^{+250}_{-230}$	BAL	41,39
PSOJ158-14	10:34:46.50	-14:25:15.58	30	6.065	19.19	18.62	18.47	-	-	-	no-BAL	42,39
PSOJ183+05	12:12:26.98	+05:05:33.49	113	6.428	19.77	19.74	20.03	-	-	-	no-BAL	43,39
PSOJ183-12	12:13:11.81	-12:46:03.45	30	5.893	19.07	18.98	19.18	540^{+200}_{-130}	$16{,}280^{+430}_{-100}$	$25{,}910^{+120}_{-330}$	BAL	39,22
PSOJ217-16	14:28:21.39	-16:02:43.30	34	6.135	19.71	18.99	19.39	-	-	-	no-BAL	39,22
PSOJ217-07	14:31:40.45	-07:24:43.30	113	6.166	19.85	19.92	19.67	$4{,}410^{+160}_{-90}$	$22{,}000^{+90}_{-150}$	$43{,}970^{+430}_{-230}$	BAL	39,39
PSOJ231-20	15:26:37.84	-20:50:00.66	37	6.564	19.66	19.91	19.97	600^{+240}_{-220}	540^{+160}_{-90}	$2{,}680^{+110}_{-130}$	BAL	44,39
J1535+1943	15:35:32.87	+19:43:20.10	36	6.358	19.63	18.55	18.46	-	-	-	no-BAL	39,39
PSOJ239-07	15:58:50.99	-07:24:09.59	164	6.114	19.37	18.94	18.65	$1{,}880^{+100}_{-110}$	810^{+110}_{-100}	$6{,}100^{+120}_{-100}$	BAL	42,39
PSOJ242-12	16:09:45.53	-12:58:54.11	15	5.840	19.71	19.00	19.50	-	-	-	no-BAL	39,22
PSOJ308-27	20:33:55.91	-27:38:54.60	85	5.799	19.46	19.63	19.37	-	-	-	no-BAL	22,22
PSOJ323+12	21:32:33.19	+12:17:55.26	103	6.585	19.74	19.06	18.97	-	-	-	no-BAL	43,22
VDESJ2211-3206	22:11:12.17	-32:06:12.94	74	6.330	19.54	18.92	18.80	$6{,}840^{+140}_{-170}$	$9{,}240^{+930}_{-100}$	$24{,}340^{+1{,}470}_{-510}$	BAL	(*),22
VDESJ2250-5015	22:50:02.01	-50:15:42.20	96	5.985	19.17	19.11	19.04	$6{,}330^{+710}_{-970}$	$22{,}500^{+110}_{-140}$	$50{,}320^{+330}_{-1{,}870}$	BAL	39,22
SDSSJ2310+1855	23:10:38.89	+18:55:19.70	161	5.992	18.86	18.50	18.75	590^{+290}_{-90}	$18{,}520^{+280}_{-1{,}030}$	$26{,}890^{+120}_{-140}$	BAL	39,22
PSOJ359-06	23:56:32.45	-06:22:59.26	154	6.169	19.85	19.26	19.04	-	-	-	no-BAL	22,22

(1) Quasar name. (2,3) Coordinates. (4) Median signal-to-noise per pixel in the 1,600–1,700 Å wavelength range, for a 50 km/s spectral binning. In the case of PSOJ242-12, two hours of observations are still needed to obtain the final spectrum. (5) Mg II-based redshift. (6) AB magnitude in the J band. (7, 8) AB magnitude in the W1 and W2 bands. (9-11) Balnicity index, minimum and maximum velocity of the C IV BAL outflows, in units of km/s. Uncertainties correspond to a 68% confidence interval. Strong (weak) BAL outflows typically have BI_0 > 1,000 km/s (BI_0 < 1,000 km/s). (12) BAL/no-BAL classification. (13) References for the J and WISE magnitudes, respectively. J magnitudes indicated with asterisks are presented herein (Methods).